Control Engineering Practice 115 (2021) 104887

Contents lists available at ScienceDirect

Control Engineering Practice

journal homepage: www.elsevier.com/locate/conengprac

Disturbance observer-based LPV feedback control of a N-DoF robotic manipulator including compliance through gain shifting

Alberto San-Miguel *, Vicenç Puig, Guillem Alenyà

Institut de Robòtica i Informàtica Industrial (CSIC-UPC), Llorens i Artigas, 4-6, 08028 Barcelona, Spain

ARTICLE INFO

Keywords:
Robotic system
Linear parameter varying
Unknown-input observer
Shifting paradigm
Robustness
Service robot

ABSTRACT

This paper proposes a control scheme for a N-DoF robotic manipulator in a joint-regulation motion problem, dealing with disturbances (as e.g. exogenous forces, unmodelled dynamics) that hinder task fulfilment, and also considering that not all the required states are available online. Existing literature tackles this problem through Disturbance Observer (DO) strategies which imply complex analysis and design methods or introducing strong assumptions. Conversely, we propose to formulate the system as a Linear Parameter Varying (LPV) model, which allows a straightforward application of the existing linear control structures but without neglecting its non-linear behaviour. We make use of the Robust Unknown Input Observer (RUIO) to obtain (for not measurable states) a decoupled estimation from the unknown disturbance effects, and improve its noise reduction capabilities through the new optimal RUIO design. The robotic manipulator is controlled with a state-feedback control law that, making use of the LPV paradigm, has been designed to seamlessly avoid torque saturation on manipulator's joints through a gain shifting strategy that modifies its compliant behaviour. Stability and performance requirements are imposed in both RUIO and state-feedback control synthesis problems stated using the LMI framework, applying Polya's theorems on positive forms of the standard simplex to reduce its overall conservatism. Experiments, using a simulated head system of the TIAGo robot as a testbed in various realistic scenarios, show the benefits when compared to the existing joint-independent PD control strategy and state-of-art EKF disturbance estimation.

1. Introduction

Leaning on the recent advances in Artificial Intelligence and Computer Vision, robotic platforms are being increasingly introduced into industrial and domestic environments, where their workspace, and even the tasks to be performed, are shared with humans. For supporting "human-in-the-loop", a key factor is to ensure their dependability under any possible scenario that might arise (Alami et al., 2006), being one of them the existence of unknown effects (disturbances) that might hinder task fulfilment. Thus, in this work, we address the motion problem of a robotic manipulator under the effect of exogenous *a-priori* unknown disturbances that should be rejected or compensated on-line. Moreover, we are going to assume that some of the required states are not measurable, as e.g. due to faulty behaviour. We are focusing on N-Degrees of Freedom (DoF) serial robotic manipulators for regulation tasks in their joint space, i.e. "point-to-point" movements.

Disturbances in robotic systems correspond to multiple phenomena from internal sources (friction, unmodelled dynamics) or interaction with the environment (collisions), presenting different behaviours and characteristics, usually non-predictable or difficult to model. Great efforts have been made within the research community to tackle this problem, some of them aiming at making the control strategy robust against disturbances (as e.g. with SMC). These strategies are defined under the category of Disturbance Observers (DO), and have been used in a wide range of platforms and for multiple purposes: from lower limb exoskeletons for estimating the exerted torque by the wearer (Mohammed, Huo, Huang, Rifaï, & Amirat, 2016) to humanoid robots to compensate for unmodelled dynamics (Bae & Oh, 2017) or even to improve boundary control approach in flexible manipulators (Zhao, Ahn and Li, 2019; Zhao & Liu, 2020). In robotic manipulators, they have been used for both single (Agarwal & Parthasarathy, 2016) and multi-agent systems (Ren, Du, Li, & Shi, 2018). Moreover, its integration with the control strategy is currently being explored, for example in Kim, Kim, Kim, Sim, and Park (2018), where it is presented as a new concept for achieving a compliant behaviour under external contacts. On the other hand, another approach is to make a design robust against disturbances (He, Wang, He, Yang, & Kaynak, 2020), but this usually involves making certain assumptions on the disturbance characteristics.

Due to the highly non-linear phenomena in robotic manipulators, the use of linear analysis and design techniques for DO has been limited to certain standard strategies, such as linearisation around

* Corresponding author.
E-mail address: asanmiguel@iri.upc.edu (A. San-Miguel).

https://doi.org/10.1016/j.conengprac.2021.104887
Received 9 November 2020; Received in revised form 2 July 2021; Accepted 6 July 2021
Available online 23 July 2021

the operating point. This is the case of the Extended Kalman Filter (EKF), which can deliver optimal performance but only if the system behaves linearly around the operation point, as in Mohammadi, Tavakoli, Marquez, and Hashemzadeh (2013). During the last decades, several techniques have emerged to deal with the control of non-linear systems, such as, e.g. Sliding Mode Control (SMC), Linear Parameter Varying (LPV) or Takagi–Sugeno (TS) gain-scheduling control, among other. In this work, we focus on the LPV paradigm (Shamma, 2012), which consist on characterising systems through a set of parameters defined by exogenous (or endogenous) signals in a gain-scheduling fashion, allowing a straightforward extension of existing linear control techniques to non-linear systems. Its success has been also motivated by the increasing use of Linear Matrix Inequalities (LMI) together with the application of Lyapunov theory to formulate multiple analysis and design problems in control (e.g. stabilisation and $\mathcal{H}_\infty$) for LPV-suitable formulations. In these cases, as including all the reachable states leads to an infinite number of constraints, LPV systems are usually described by confining all the possible trajectories of the varying parameters defined by a set of vertices, leading to the polytopic LPV formulation that considers only a family of vertex systems. Polytopic LPV together with LMI provide a systematic approach to guarantee off-line certain properties, in contrast to *ad hoc* construction of Lyapunov candidates and trial and error tuning of the controller parameters required by other non-linear control techniques (Zhao, He and Ahn, 2019).

DO exploit all the measurements that can describe the state of the system, but, as any physical entity, robots might be subjected to disturbances that affect the closed-loop behaviour. Control literature has provided many model-based observers to estimate non-available information, but in the case of system disturbances, the technique has to be robust enough against their effects. A well-known approach is to assume the dynamics of the disturbance (Ha & Back, 2019), but, in a discrete-time domain, its effectiveness is affected by the sampling period. Considering that this work aims at being applied to real robotic platforms that operate in discrete time, we will study the application of Unknown Input Observers (UIO) structures, which can obtain a state estimation disregarding the effect of disturbances and without *a-priori* assuming its behaviour.

Therefore, in this work, we aim at providing a solution to the disturbance rejection problem considering a LPV formulation of a N-DoF serial manipulator. This allows extending linear theory for analysing and designing structures for a non-linear system, which, up to our knowledge, has not been performed for disturbance rejection problems in robotic platforms. Solutions provided in the literature rely on model linearisation or neglecting non-linear dynamic terms, as e.g. in Kim et al. (2018). Considering that not all the system states are measurable on-line, we have explored the Robust-UIO formulation (RUIO for short) from Chadli and Karimi (2012) to provide a decoupled state estimation from the disturbance effects. Using this estimation, a model-based DO generates a compensating feed-forward action within the control scheme. To enhance its performance, RUIO noise reduction properties have been improved through a novel formulation of its LMI design problem based on Kalman Riccati equations. To completely address the motion regulation problem, we have described the synthesis of an optimal state-feedback controller through the Linear Quadratic Regulator (LQR) LMI problem. Additionally, we have introduced a gain shifting strategy (Rotondo, Nejjari and Puig, 2015) aimed at seamlessly modifying control compliance to avoid joint torque saturation effects (which represents a worst-case scenario for the feedforward compensation of disturbances).

It should be pointed out that the LPV paradigm has not been widely applied to robotics yet, mainly due to the large number of varying parameters of the generated models. These issues are tackled within the LPV literature from two different perspectives: (1) by increasing the flexibility of problem constraints and/or (2) by modifying the model used. Latter ones consist on reducing over-boundness of the LPV model description by reshaping the set of varying parameters according to their behaviour (Bruzelius, Breitholtz, & Pettersson, 2002) or approximating the system to an LPV model with a reduced number of parameters as e.g. in Hashemi, Abbas, and Werner (2012), which is also one of the few application examples of LPV techniques in robotic manipulators. On the other hand, reducing problem conservatism by relaxing constraints lies in state-of-art methods from the field of mathematics, usually trading-off an increase in the number of constraints. In this work, we propose to further exploit the use of these techniques in robotic applications by making use of Polya's theorems (Sala & Arino, 2007) in both the RUIO and state-feedback controller LMI synthesis problems.

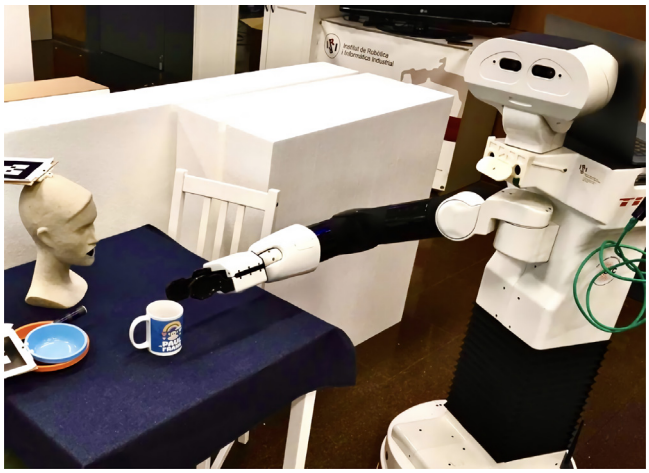

Fig. 1. TIAGo robotic platform developed by PAL Robotics performing a manipulation task.

This paper is organised as follows: Section 2 describes the LPV modelling of the manipulator and its polytopic representation. Section 3 is devoted to the estimation of exogenous force effects using state variables. The improved formulation of the RUIO and the derivation of design conditions to minimise noise effects are presented in Section 4, together with the introduction of Polya's theorems for its synthesis problem. In Section 5, the shifting control paradigm and its formulation under Polya's method are described. Section 6 illustrates the application of the complete approach to the head of TIAGo robot, providing simulation results under different settings. The final section concludes the presented work and highlights future research developments.

2. System modelling

2.1. Description

The TIAGo humanoid robot (Fig. 1) developed by PAL Robotics[1] has been used in this paper to exemplify the described methodology and techniques. This robotic platform is meant to operate in both domestic and industrial anthropic domains as a service robot, featuring a wide set of capabilities related with navigation, perception and human–robot interaction, making it suitable for research purposes. It is also fully-integrated within the well-known Robotic Operating System (ROS) ecosystem,[2] which offers realistic simulations through Gazebo[3] using the same communication interface for controlling the real robot.

Particularly, the focus has been put in the 2-DoF TIAGo head system. This responds to an existing issue with its pose control strategy,

[1] TIAGo robotic platform by PAL Robotics: http://tiago.pal-robotics.com/ (Accessed August 18, 2021).

[2] ROS software development framework for robotics https://www.ros.org/ (Accessed August 18, 2021).

[3] Gazebo http://gazebosim.org/ simulator for robotic applications (Accessed August 18, 2021).

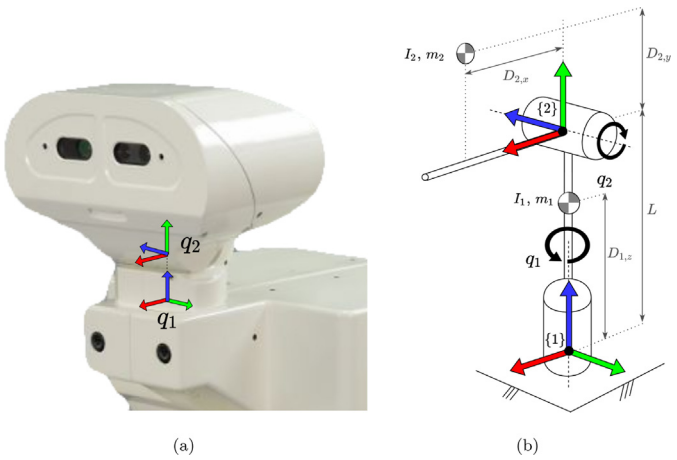

(a) (b)

Fig. 2. Head subsystem of the TIAGo robotic platform (a), represented as a two-manipulator link (b).

Table 1
Description and value of inertial and distance parameters of the TIAGo head subsystem.

Parameter	Description	Value
I_1	Inertial tensor of first link	$\text{diag}(1.192, 1.402, 0.889) \cdot 10^{-3}$ [kg m^2]
I_2	Inertial tensor of second link	$\text{diag}(4.620, 4.861, 3.132) \cdot 10^{-3}$ [kg m^2]
m_1	Mass of first link	0.622 [kg]
m_2	Mass of second link	0.661 [kg]
L	Dist. in ${}^1\hat{Z}_1$ between {1} and {2}	0.098 [m]
$D_{1,z}$	Dist. of CoG_1 in ${}^1\hat{Z}_1$ w.r.t. {1}	0.072 [m]
$D_{2,x}$	Dist. of CoG_2 in ${}^2\hat{X}_2$ w.r.t. {2}	0.047 [m]
$D_{2,y}$	Dist. of CoG_2 in ${}^2\hat{Y}_2$ w.r.t. {2}	0.055 [m]

based on joint-independent PD control, which was not able to reach desired positions when a device (e.g. an additional RGB-D camera) was attached, i.e. under the effect of a force associated to a mass. Head positioning is crucial to ensure the required vision and 3D mapping features of the TIAGo robot, becoming paramount to overcome this issue. Either way, a valid description of the methods is given in this work for any N-DoF mechanism with rotational joints, such as a serial robotic manipulator.

2.2. Analytical model

As any model-based approach, a set of analytical expressions that describe the behaviour of the system has to be determined. For any N-DoF robotic manipulator with rotational joints, applying well-known Newton–Euler formulation (Craig, 2009), joint torque vector τ can be defined as a function of the joint acceleration $\ddot{q}$, velocity $\dot{q}$ and position q vectors:

$$\tau = \mathbf{M}(q)\,\ddot{q} + \mathbf{B}(q)\,[\dot{q}\dot{q}] + \mathbf{C}(q)\,[\dot{q}^2] + \mathbf{G}(q) \tag{1}$$

where $\mathbf{M}(q) \in \mathbb{R}^{N\times N}$ is the mass matrix, $\mathbf{G}(q) \in \mathbb{R}^N$ the gravity effects, $\mathbf{C}(q) \in \mathbb{R}^{N\times N}$ the centrifugal coefficients, and $\mathbf{B}(q) \in \mathbb{R}^{N\times N(N-1)/2}$ the Coriolis terms. Joint friction phenomenon has been considered as *a-priori* modelled, such that their influence on the control scheme is either fully cancelled or minimised (being a source of system noise in this latter case), and therefore it has been be omitted in Eq. (1). This assumption has been made considering that there exist several techniques that, from different approaches, successfully tackle this problem as e.g. in Colomé, Planells, and Torras (2015).

Following the guidelines included in Appendix A for the TIAGo head system, depicted in Fig. 2 along with its abstracted link scheme, we obtain the terms of Eq. (1):

$$\mathbf{M}(q) = \begin{bmatrix} I_{zz_1} + m_2(s_2 D_{2,y} - c_2 D_{2,x})^2 + I_{xx_2} s_2^2 + I_{yy_2} c_2^2 & 0 \\ 0 & I_{zz_2} + m_2(D_{2,x}^2 + D_{2,y}^2) \end{bmatrix}, \tag{2a}$$

$$\mathbf{B}(q) = \begin{bmatrix} 2m_2(s_2 D_{2,x} + c_2 D_{2,y})(s_2 D_{2,y} - c_2 D_{2,x}) + 2(I_{xx_2} - I_{yy_2}) s_2 c_2 \\ 0 \end{bmatrix}, \tag{2b}$$

$$\mathbf{C}(q) = \begin{bmatrix} 0 & 0 \\ m_2(c_2 D_{2,x} - s_2 D_{2,y})(s_2 D_{2,x} + c_2 D_{2,y}) & 0 \end{bmatrix} \tag{2c}$$

$$\mathbf{G}(q) = \begin{bmatrix} 0 \\ m_2(c_2 D_{2,x} - s_2 D_{2,y}) g \end{bmatrix} \tag{2d}$$

being c_i and s_i abbreviations for $cos(q_i)$ and $sin(q_i)$, respectively, and g for the Earth gravity constant. Regarding remaining parameters, I_{a_i} represent inertial tensor term on the $a = \{x, y, z\}$ axis for the ith link, m_i the mass of the ith link and $D_{2,a}$ the distance along axis a from the base of frame {2} of to the CoG_2, all in SI units. The value of these parameters are given by the manufacturer and have been gathered in Table 1.

2.3. LPV model

As proposed in Kwiatkowski, Boll, and Werner (2006), non-linearities can be embedded within varying parameters using the LPV paradigm. This technique provides an exact representation of the original non-linear system (1), and its applicability is constrained to the following set of conditions $\forall i = \{1, \dots, n_{\Phi}\}$:

1. Varying parameter $\phi_i(x_1, \dots, x_{n_x})$ has to be bounded in $[\underline{\phi_i}, \overline{\phi_i}]$ for the (bounded) variable set $\{x_1, \dots, x_{n_x}\}$ and continuous within this interval.
2. Controllability of the system has to be ensured for any value of ϕ_i.

From Eq. (1), expressions for joint angular accelerations can be obtained as function of joint velocities, positions and torques. Without loss of generality, considering a state vector $x(t) = [\dot{q}_1, \dot{q}_2, \dots, \dot{q}_N, q_1, q_2, \dots, q_N]^T$, and the joint torque vector $u(t) \equiv \tau(t)$, the following state–space alike representation can be obtained

$$\dot{x}(t) = A^c(x(t))\,x(t) + B^c(x(t))\,u(t) + \mathfrak{g}^c(x(t)), \tag{3}$$

where

$$\mathcal{A}^c(x(t))\,x(t) = -\mathbf{M}(q)^{-1}\begin{bmatrix}(\mathbf{B}(q)[\dot{q}\dot{q}] + \mathbf{C}(q)[\dot{q}^2]) \\ 0_{2N\times N}\end{bmatrix} + \begin{bmatrix}0_{N\times N} & 0_{N\times N} \\ I_{N\times N} & 0_{N\times N}\end{bmatrix} x(t)$$

$$\mathbf{B}^c(x(t)) = [-\mathbf{M}(q)^{-1} \quad 0_{N\times N}]^T$$

$$\mathfrak{g}^c(x(t)) = [-\mathbf{M}(q)^{-1}\,\mathbf{G}(x(t)) \quad 0_{N\times 1}]^T.$$

Note that using this formulation, state matrix $A^c(t)$ has not a straightforward definition decoupled from $x(t)$, due to Coriolis and Centrifugal effects. Therefore, its definition is not unique and has to be made *a-posteriori* on Eq. (1) applied to each particular system. Subscript "c" denotes matrices for continuous-time systems, meaning its absence that they correspond to discrete-time forms.

Eq. (3) corresponds to a state–space alike formulation where state and input matrices A^c and B^c, respectively, depend on state vector $x(t)$. LPV framework formalises this type of systems by considering state–space matrices as function of a set of varying parameters $\boldsymbol{\Phi} \in \mathbb{R}^{n_{\Phi}}$ that are function of some scheduling variables that are on-line measured or estimated.

Regarding the TIAGo head system, from the joint configuration space described in (2a)–(2d), its state–space alike representation arises:

$$A^c(q_2, \dot{q}_1) = \begin{bmatrix} 0 & \frac{B_{(1,1)}(q_2)}{\mathbf{M}_{(1,1)}(q_2)}\dot{q}_1 & 0 & 0 \\ \frac{\mathbf{C}_{(2,1)}(q_2)}{\mathbf{M}_{(2,2)}}\dot{q}_1 & 0 & 0 & 0 \\ 1 & 0 & 0 & 0 \\ 0 & 1 & 0 & 0 \end{bmatrix},$$

$$B^c(q_2) = \begin{bmatrix} 1/\mathbf{M}_{(1,1)}(q_2) & 0 \\ 0 & 1/\mathbf{M}_{(2,2)} \\ 0 & 0 \\ 0 & 0 \end{bmatrix}, \qquad \mathfrak{g}_v^c(q_2) = \begin{bmatrix} \frac{\mathbf{G}_{(2,1)}(q_2)}{\mathbf{M}_{(2,2)}} \\ 0 \\ 0 \\ 0 \end{bmatrix},$$

Table 2
State, input torque and scheduling variables limits for TIAGo head subsystem.

Variable	Minimum	Maximum
$\dot{q}_i$ [rad/s]	−3	3
q_1 [°]	−75	75
q_2 [°]	−60	45
τ_i [N m]	−6	6
ϕ_1	0.0055	0.0091
ϕ_2	−0.0110	0.0110

where $X_{(i,j)}$ refers the element of matrix X in the ith row and j-column. Notice that from the comparison between (2b) and (2c), a further simplification can be made by considering $\mathbf{B}_{(1,1)}(q_2) = -2\mathbf{C}_{(2,1)}(q_2)$. Thus, the scheduling variables have been defined as follows:

$$\boldsymbol{\Phi} \triangleq [\phi_1,\ \phi_2] = [\mathbf{M}_{1,1}(q_2),\ \mathbf{C}_{2,1}(q_2)\dot{q}_1]. \tag{4}$$

Bounds for ϕ_i can be obtained from the state variables limits, also given by the operation conditions of the TIAGo robot, both listed in Table 2. Conditions for non-linear embedding method are held for this definition of $\boldsymbol{\Phi}$: (1) ϕ_i are bounded considering the limits of state variables, (2) controllability property depends only on the selection of the output model, which will be addressed in Section 4, as matrix A does not lose rank for any value of ϕ_i.

Remark 1. It is worth to remark that the selection of $\boldsymbol{\Phi}$ is generally made (and so in this work for the TIAGo head example) such that the minimal set of scheduling variables is obtained, as the polytopic reconstruction has a complexity that grows with $\mathcal{O}(2^{n_\phi})$. As aforementioned, further methods and criteria can be applied to reduce the complexity of a LPV polytopic representation of a system through the reduction on the number of varying parameters, obtaining an approximated representation of the system.

Remark 2. In LPV literature, if any of the varying parameters is function of endogenous variables, the model is formally denoted as *quasi*-LPV. Although this is the case for the considered N-DoF manipulator whose $\boldsymbol{\Phi}$ set is defined according to joint position and velocities, throughout this work we refer to LPV to avoid misleading interpretations for non-expert readers.

2.4. Polytopic LPV model

In order to get the presented techniques closer to their implementation on a real robotic manipulator, all of them have been designed for the discrete-time domain. According to Toth, Heuberger, and Van den Hof (2010), the discrete-time form of a continuous-time LPV model can be obtained if system's matrices have been evaluated according to a discretisation method for a sampling time T_s. More details on the discrete-time implementation are given in Section 6.

Considering the discrete-time form of (3), the LPV representation of the system is the following one:

$$x(k+1) = A(\boldsymbol{\Phi})\,x(k) + B(\boldsymbol{\Phi})\,u(k). \tag{5}$$

Regarding gravity effects $\mathfrak{g}^c(x(k))$ in (3), they appear as an independent term and will be omitted for the upcoming modelling process, considering that in our approach this term is counteracted through a feed-forward action, which will be addressed in Section 3.

In order to avoid considering all the reachable states for the LPV system, all the possible trajectories of $\boldsymbol{\Phi}$ can be confined in a polytope Ω defined by a set of vertices:

$$\boldsymbol{\Phi}(k) \in \Omega := Co\{\omega_1, \dots, \omega_n\} \tag{6}$$

being $n = \{1, \dots, 2^{n_\Phi}\}$. Thus, the state–space matrices are confined in the polytope defined by their image at these vertices:

$$\begin{bmatrix} A(\boldsymbol{\Phi}) & B(\boldsymbol{\Phi}) \end{bmatrix} \in Co\left\{ \begin{bmatrix} A_n & B_n \end{bmatrix} := \begin{bmatrix} A(\omega_n) & B(\omega_n) \end{bmatrix} \right\}. \tag{7}$$

Using this approach, system representation Eq. (5) can be stated as a weighted function of their images on polytope vertex as follows:

$$x(k+1) = \sum_{n=1}^{2^{n_\Phi}} \mu_n(\boldsymbol{\Phi})[A_n(\boldsymbol{\Phi})x(k) + B_n(\boldsymbol{\Phi})u(k)] \tag{8}$$

where $\mu_n(\boldsymbol{\Phi})$ are the polytopic coefficients, such that:

$$\sum_{n=1}^{2^{n_\Phi}} \mu_n(\boldsymbol{\Phi}) = 1, \quad \mu_n(\boldsymbol{\Phi}) \geq 0 \tag{9}$$

From the set of applicability conditions, we know that $\phi_i \in [\underline{\phi}_i, \overline{\phi}_i]$, and so the set of vertices will correspond to all the possible combination of these limits. Thus, $\mu_n(\boldsymbol{\Phi})$ can be defined as

$$\mu_n(\boldsymbol{\Phi}) = \prod_{m=1}^{n_\Phi} \xi_{nm}(\eta_0^m, \eta_1^m) \tag{10}$$

where,

$$\xi_{nm}(a,b) = \begin{cases} a & \text{if} \quad mod(n, 2^m) \in \{1, \dots, 2^{m-1}\} \\ b & \text{else} \end{cases}$$

considering a linear interpolation between the limits.

3. Model-based DO

This work aims at obtaining a control structure that is able to adapt its behaviour according to an exogenous disturbance such that it does not interfere the task fulfilment and/or some undesired effects are avoided. Particularly, a robotic mechanism is meant to track certain joint trajectories and might be affected by an external force $\mathcal{F}$ at any time, which will (presumably) hinder this task. Therefore, the chosen strategy is to compensate its effects such that an admissible tracking performance is obtained, which requires of their estimation through a DO.

Recalling the joint configuration space in Eq. (1), $\mathcal{F}$ will exert a set of joint torques $\tau_\mathcal{F}$:

$$\tau + \tau_\mathcal{F} = \mathbf{M}(q)\,\ddot{q} + \mathbf{N}(q,\dot{q}) + \mathbf{G}(q) \tag{11}$$

modifying Eq. (5) as follows:

$$x(k+1) = A(\boldsymbol{\Phi})\,x(k) + B(\boldsymbol{\Phi})\,(u(k) + \tau_\mathcal{F}(k)). \tag{12}$$

Following a similar approach than the one proposed in Witczak (2014) for fault estimation, and considering the discrete-time difference between current system state $x(k)$ at time instant k and the expected value given by the available model of the system considering previous state $x(k-1)$ using Eq. (12), the exerted torque can be estimated as follows

$$\begin{aligned} \tau_\mathcal{F}(k-1) = B^\dagger(k-1)[x(k) - A(\boldsymbol{\Phi}(k-1))\,x(k-1) \\ + B(\boldsymbol{\Phi}(k-1))\,u(k-1)], \end{aligned} \tag{13}$$

where $B^\dagger$ represents the pseudoinverse of matrix B. Note that using the available information at time step k it is only possible to obtain $\tau_\mathcal{F}$ at time instant $k-1$. This is often solved in the literature considering that $\tau_\mathcal{F}(k) = \xi\,\tau_\mathcal{F}(k-1)$, where the term ξ corresponds to a gain design parameter. In this work, it has been considered equal to a identity matrix, i.e. a one time-step predictor.

It is worth to mention that through this approach $\tau_\mathcal{F}(k)$ is generated using joint position and velocities from the system, considering the available sensors on the TIAGo head system (and the vast majority of robotic mechanisms)

4. State estimation

As the generation of $\tau_{\mathcal{F}}(k)$ depends on the system states, these measurements have to be available online during the complete execution of a task. Although this premise is generally accepted, the robotics community points out that as robotic platforms have to operate uninterruptedly during long periods, and considering their inherent complexity, they are prone to different types of adverse events that should be overcome. Thus, in this work we have extended the problem to consider a limited number of measurements during the whole task. In the particular case of the TIAGo head, system output y has been considered as follows:

$$y = C\,x = [\dot{q}_2, q_1, q_2]^T. \tag{14}$$

where matrix $C \in \mathbb{R}^{n_y \times n_x}$. In this case, C is constant disregarding the operating point of the system, so no LPV formulation is required. Recalling the conditions described in Section 2 to define the scheduling vector Φ through the non-linear embedding approach, the given definition of C ensures the observability property for any value of ϕ_i.

4.1. Robust unknown input observer

The UIOs allow to obtain a decoupled estimation from the effects of an unknown input, disregarding its behaviour. Particularly, the Robust-UIO for Takagi–Sugeno models (RUIO for short) presented in Chadli and Karimi (2012) has been adapted to this problem, making use of existing strong analogies between Takagi–Sugeno and polytopic LPV representation (Rotondo, Puig, Nejjari and Witczak, 2015).

The RUIO assumes the following polytopic LPV discrete-time state–space representation

$$x(k+1) = \sum_{n=1}^{2^{n_\Phi}} \mu_n(\Psi)[A_n x(k) + B_n u(k) + R_n f(k)], \tag{15a}$$

$$y(k) = C\,x(k), \tag{15b}$$

where $f(k) \in \mathbb{R}^{n_f}$ stands for the unknown input vector, being n_f the number of unknown inputs considered. Matrix $R_n \in \mathbb{R}^{n_x \times n_f}$ represents the influence of $f(k)$ in the system behaviour. These matrices are determined according to the desired effect to represent, and provide the existence of a solution as described in Chadli and Karimi (2012). Recalling the state–space form including the exerted torque from Eq. (12) and defined output model in Eq. (14):

$$R_n \triangleq B_n.$$

The structure for the RUIO is:

$$z(k+1) = \sum_{n=1}^{2^{n_\Phi}} \mu_n(\Phi)[N_n z(k) + G_n u(k) + L_n y(k)] \tag{16a}$$

$$z(k) = \hat{x}(k) + E y(k) \tag{16b}$$

where $z(k)$ corresponds to RUIO's state vector, with the same dimensions of $x(k)$, which embeds the given estimation $\hat{x}(k)$. Matrices N_n, G_n, L_n and E are the observer gains to be designed by ensuring an asymptotic stability of the observer dynamics, i.e. the estimation error converges to zero as time tends to infinite disregarding the unknown inputs magnitude. Fig. 3 graphically represents the RUIO structure within the complete architecture.

Remark 3. The original formulation from Chadli and Karimi (2012) does differentiate between "unknown inputs" and "disturbances". In this paper, we refer to the first type as either "disturbances" or "unknown inputs", and the second type corresponds to "noise". We use this nomenclature to help the reader link these terms to the real implementation.

4.2. Optimal RUIO

One of the main contributions of this work is the introduction of conditions for optimal design based on Riccati equations of the Kalman filter for the RUIO. In the application to the real platform, process and sensor noise cannot be avoided, therefore their effects have to be minimised such that do not hinder the estimation of the unknown states. This formulation allows to introduce process and sensor noise covariance through matrices Q_o and R_o, that define the quadratic criterion J_o according to the estimation error $e(k) = x(k) - \hat{x}(k)$:

$$J_o = \sum_{k=0}^{\infty} (e(k)^T\, Q_o\, e(k) + e^T(k)\, K_i C\, R_o\, C^T K_i^T\, e(k)) < \gamma_o \tag{17}$$

Proposition 1 (*Optimal RUIO Design*). *Given $Q_o = Q_o^T = H_o^T H_o > 0$ and $R_o = R_o^T > 0$ matrices, and the optimal performance upper bound $\gamma_o > 0$, the observer from Eq. (16) converges asymptotically to the state of the polytopic discrete-time LPV model from Eq. (15) if there exists matrices sets*

$$\mathbf{X} = \{X_1, \dots, X_{2^{n_\Phi}}\};\ X_n \in \mathbb{R}^{n_x \times n_x} \mid X_n = X_n^T > 0 \quad \forall n = 1, \dots, 2^{n_\Phi}, \tag{18a}$$

$$\mathbf{W} = \{W_1, \dots, W_{2^{n_\Phi}}\};\ W_n \in \mathbb{R}^{n_x \times n_y}, \tag{18b}$$

$$\mathbf{S} = \{S_1, \dots, S_{2^{n_\Phi}}\};\ S_n \in \mathbb{R}^{n_x \times n_y}, \tag{18c}$$

such that the following conditions hold $\forall \vec{i} \in \mathbb{I}_{(2,2^{n_\Phi})}$:

$$\begin{bmatrix} -X_{i_1} & X_{i_1}A_{i_1} + S_{i_1}CA_{i_1} - W_{i_1}C & X_{i_1}H_o^T & W_{i_1} \\ (*) & -X_{i_2} & 0 & 0 \\ (*) & 0 & -I & 0 \\ (*) & 0 & 0 & -R_o^{-1} \end{bmatrix} < 0, \tag{19a}$$

$$(X_{i_1} + S_{i_1}C)R_{i_1} = 0, \tag{19b}$$

$$\begin{bmatrix} \gamma_o I & I \\ I & X_{i_1} \end{bmatrix} > 0 \tag{19c}$$

where the symbol $(*)$ denotes the transpose of the element in the symmetric position, and

$$\mathbb{I}_{(r,h)} = \{\vec{i} = (i_1, \dots, i_r) \in \mathbb{N}^r \mid 1 \le i_n \le h \quad \forall n = 1, \dots, r\}.$$

The obtained solution for these matrices defines RUIO's gains for $n = 1, \dots, 2^{n_\Phi}$:

$$E = X_n^{-1} S_n, \tag{20a}$$

$$G_n = (I + X_n^{-1} S_n C) B_n, \tag{20b}$$

$$N_n = (I + X_n^{-1} S_n C) A_n - X_n^{-1} W_n C, \tag{20c}$$

$$L_n = X_n^{-1} W_n - N_n E_n. \tag{20d}$$

Proof. The proof is given in Appendix B.

Note that $\mathbb{I}_{(r,h)}$ is a multi-index notation to represent all the combinations of h elements that can take (natural) values from 1 to r. Therefore, $\mathbb{I}_{(2,2^{n_\Phi})}$ represents all the possible pairwise combinations between the 2^{n_Φ} vertex imposed by RUIO condition in Eq. (19a). For the N-DoF mechanism case, the number of states $n_x = 2N$, and remaining terms are defined by the number of varying parameters and the chosen output model.

4.3. Polya's theorems formulation for the RUIO

In the proposed extension of the RUIO method including optimality conditions, some feasibility issues could arise depending on the number of polytope vertices and the similarity between them (i.e. the variability in terms of the scheduling parameters image). Also equality constraints from Eq. (19b) have been found to highly increase complexity of the overall problem, as it imposes a strict relation between terms. Although a set of positive definite variables $\mathbf{X} = \{X_1, \dots, X_n\}$ has been

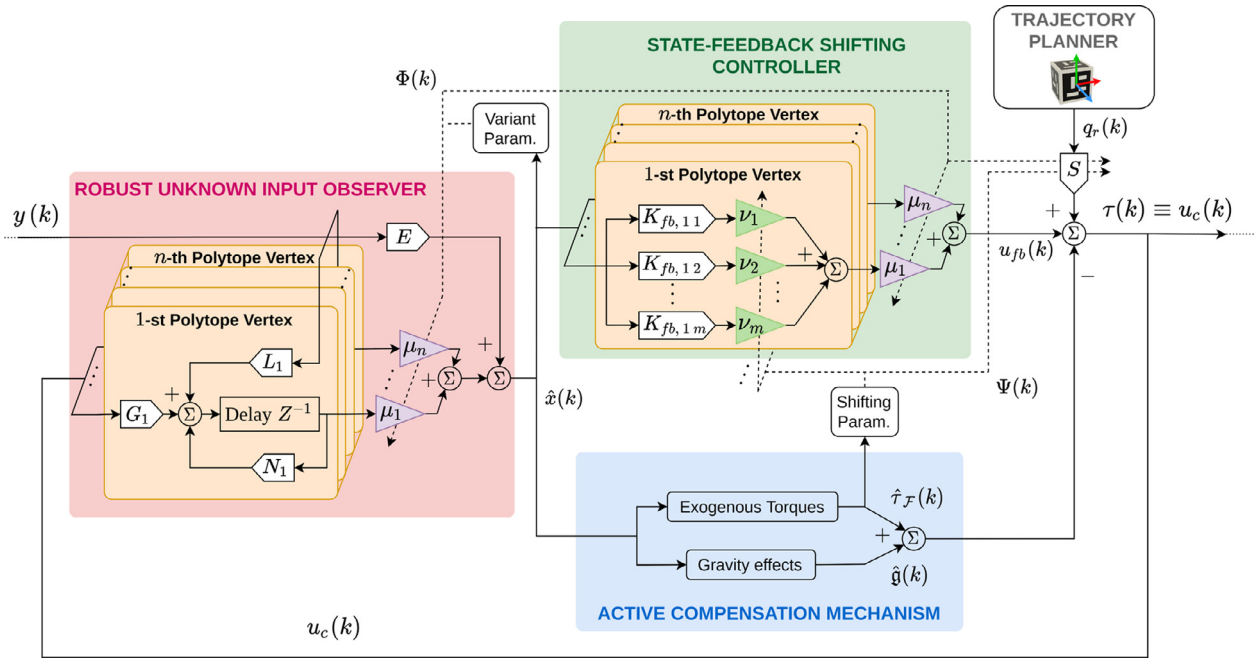

Fig. 3. Schematic representation of the complete control architecture for the polytopic LPV formulation of the TiaGO head system, including the Robust Unknown Input Observer (RUIO), the State-feedback Shifting Control and Active Compensation strategies.

included in the formulation to reduce overall problem conservatism, we have additionally applied Polya's theorems on positive forms of the standard simplex to obtain sufficient conditions, as proposed by Sala and Arino (2007). This solution introduces a new set of constraints through dimensionality expansions of the LMI conditions. These new inequalities are obtained as sums of matrices evaluated in a certain index combination according to a multi-index vector in $\mathbb{I}_{(r,2^{n_\Phi})}$, where r represents a *complexity parameter* of the method: larger values imply greater number of conditions, increasing the associated computation burden but reducing the overall conservatism of the problem. A brief description of the method has been included in Appendix C. Thus, combinatorial constraints from Eq. (19a) can be substituted by the following one for a given $r \geq 2$:

$$\sum_{\vec{j}\in\mathcal{P}(\vec{i})} \begin{bmatrix} -X_{j_1} & X_{j_1}A_i + S_{j_1}CA_{j_1} - W_{j_1}C & X_{j_1}H_o^T & W_{j_1} \\ (*) & -X_{j_2} & 0 & 0 \\ (*) & 0 & -I & 0 \\ (*) & 0 & 0 & -R_o^{-1} \end{bmatrix} < 0$$
$$\forall \vec{i} \in \mathbb{I}^{+}_{(r,2^{n_\Phi})} \tag{21}$$

5. Shifting control design

5.1. Feedback control law

The RUIO gives a decoupled estimation for system states from the effects of an unknown exogenous force exerted on the system, allowing to use an state-feedback control strategy. For the polytopic discrete-time LPV system, which can be derived from Eq. (8), the corresponding state-feedback control law is:

$$u_{fb}(k) = -K_{fb}(\boldsymbol{\Phi})\,\hat{x}(k) = -\sum_{n=1}^{2^{n_\Phi}} \mu_n(\boldsymbol{\Phi}) K_{fb,n}\,\hat{x}(k). \tag{22}$$

Joint trajectory references are assumed to be given by an external planning module, according to a specific high-level objective, as e.g. for the TIAGo head system, an object tracking algorithm based on live-image input. Associated control actions to the trajectory references has been computed by means of the Feedforward Scaling matrix $S(\boldsymbol{\Phi})$, defined for the considered system:

$$S(\boldsymbol{\Phi}) = \sum_{n=1}^{2^{n_\Phi}} \mu_n(\boldsymbol{\Phi})[C_r\,(I + B_n\,K_{fb,n} - A_n)^{-1}\,B_n]^{-1}. \tag{23}$$

Note that matrix C_r is determined considering the system states to be regulated through the control law, in this case, joint reference positions given by vector $q_r(k) = [q_1(k), \ldots, q_N(k)]^T$. Thus, the input control action u_c for the system can be obtained as

$$u_c(k) = u_{fb}(k) + S(\boldsymbol{\Phi})q_r(k). \tag{24}$$

Besides stability, control gains can be obtained according to certain criteria regarding desired performance. Also from the Riccati equations, the well-known quadratic optimal control, referred in the literature as Linear Quadratic Regulator (LQR) problem, aims at obtaining a controller according to the quadratic index J_c similarly defined as in Eq. (17)

$$J_c = \sum_{k=0}^{\infty} (x(k)^T\,Q_c\,x(k) + x^T(k)\,K_{fb}\,R_c\,K_{fb}^T\,x(k)) < \gamma_c. \tag{25}$$

There is not a straightforward definition to be considered for tuning of Q_c and R_c like in the observer synthesis problem. Generally, LQR design approach is used to reduce the oscillatory behaviour of the system response by penalising the magnitude increase of states and control actions. In this work, it has been done through a weighted Bryson's Rule, which gives their definition according to the squared maximum admissible values of variables $\overline{d}_i$ and user-defined weights δ_i:

$$Q_c = \text{diag}\left\{\frac{\delta_1}{\overline{d}_1}, \quad \cdots \quad, \frac{\delta_{2N}}{\overline{d}_{2N}}\right\}, \quad R_c = \text{diag}\left\{\frac{\delta_{2N+1}}{\overline{d}_{2N+1}}, \ldots, \frac{\delta_{2N+n_u}}{\overline{d}_{2N+n_u}}\right\}, \tag{26}$$

where n_u corresponds to the number of control inputs for the system. The selection of $\overline{d}_i$ has been done for the TIAGo Head system recalling the limits imposed by the real platform and summarised in Table 2 for state variables and control input actions. The selection of δ_i will be detailed in Section 6.1, as it corresponds to a tuning procedure on the system.

Remark 4. Bryson's rule defines Q_c and R_c on *desirable* maximum admissible values, as LQR conditions do not restrict state and action

values but allow design the controller ensuring stability according to J.

5.2. Active compensation and shifting paradigm

As aforementioned, the set of torques exerted by the exogenous force $\hat{\tau}_F$ is meant to be actively compensated without jeopardising task fulfilment. Recalling the state–space alike representation from Eq. (3), gravity effects denoted by $\mathfrak{g}$ where omitted to construct the polytopic LPV model, on the assumption that this term will be also counteracted. Thus, using the decoupled state estimation computed by the RUIO $\hat{x}(k)$, the counter values of both $\hat{\tau}_F$ and $\hat{\mathfrak{g}}$ can be obtained and actively injected in u_c such that joint torque vector τ is generated:

$$\tau(k) \equiv u(k) = u_c(k) - [\hat{\tau}_F(k) + \hat{\mathfrak{g}}(k)]. \tag{27}$$

Active compensation relieves the state-feedback control strategy of generating the required effort to simultaneously track desired joint trajectories and compensate for additional effects. This allows to ensure some stability and desirable performance properties on the controller synthesis problem, considering the nominal operation instead of all the possible ones that might arise from the effects of unknown inputs, which in practice will not be tractable. However, this paradigm underlies the assumption that control strategy and compensation mechanism can operate individually disregarding any further constraint implying both of them. In this work, we have considered actuator saturation, which imposes that the control torque $\tau(k)$ obtained as the sum of both the active compensation and state-feedback actions has to be bounded in order to avoid ill-posing control performance and stability, or damaging the actuator itself. Therefore, we have introduced a design strategy where the controller acknowledges this saturation effects by adapting control compliance according to the magnitude of the effects to be compensated, following the *shifting paradigm* as applied by Ruiz, Rotondo, and Morcego (2019).

This paradigm for LPV formulations considers an augmentation of the varying parameter set $\boldsymbol{\Phi}$ with a new one $\boldsymbol{\Psi} \in \mathbb{R}^{n_\Psi}$, henceforth referred as shifting parameter set, used to alter the state-feedback control law behaviour in Eq. (22) as follows

$$u_{fb} = -K_{fb}(\boldsymbol{\Phi})\,\hat{x}(k) = -\sum_{n=1}^{2^{n_\Phi}} \mu_n(\boldsymbol{\Phi}) \sum_{m=1}^{2^{n_\Psi}} \nu_m(\boldsymbol{\Psi}) K_{fb,nm}\,\hat{x}(k) \tag{28}$$

where $\nu_m(\boldsymbol{\Psi})$ are the associated polytopic weights defined following conditions from Eq. (9). This structure has been also graphically depicted within the complete control architecture in Fig. 3. Shifting variables have to be defined considering the phenomena on which the control behaviour has to be modified, in this particular case, the magnitude of the compensated effects with respect to the torque limits. Defining the input saturated action for the ith actuator

$$u_i = \begin{cases} \text{sign}(u_i)\,\overline{u}_i & \text{if} \quad \text{abs}(u_i) > \overline{u}_i \\ u_i & \text{if} \quad \text{abs}(u_i) \le \overline{u}_i, \end{cases} \tag{29}$$

where $\overline{u}_i$ is the saturation limit (assuming a symmetry on the effect), shifting variable ψ_i is defined according to the difference between the exerted torque and gravity effects and input saturation limits, scaled such that $\psi_i \in [0, 1]$:

$$\psi_i = \frac{\overline{u}_i^2 - [\hat{\tau}_F(k) + \hat{\mathfrak{g}}(k)]^2}{\overline{u}_i^2}. \tag{30}$$

Defining the behaviour associated with the shifting strategy relies on the synthesis problem of state-feedback gains $K_{fb,nm}$. Following the polytopic approach, different performances have to be associated with the limits of ψ_i such that any value within these bounds has the corresponding "interpolated" one. To avoid reaching actuator saturation limits, it is desired that as the corresponding torque of the actively compensated effects increases, the state-feedback control compliance is increased, i.e. control effort is decreased through a slower response of the closed-loop system. Control theory has proven for the LPV systems the influence of placing the system's poles in some particular regions on the performance characteristics (Ruiz et al., 2019). Particularly, system response can be defined by its time constant $\boldsymbol{\tau}_s$, for a given sampling time T_s, which can be determined by the magnitude of its poles. Thus, in this work, pole placement conditions that constraint poles to certain regions have been introduced into the control synthesis problem to define the system response, depending on the values of shifting variables.

In order to ease a straightforward applicability of this method, pole placement has been defined in circular regions according to the settling time of the system $T_{sett,\kappa}$ for a certain band with a width of $\kappa\%$ reference value. Thus, given desired maximum and minimum values, respectively $\overline{T}_{sett,\kappa\%}$ and $\underline{T}_{sett,\kappa\%}$, their radii ρ_k and centre σ_k in the complex plane can be defined as follows $\forall k = 1, \dots, 2^{\Psi}$:

$$\rho_k = \frac{e^{-\alpha_k T_s} - e^{-\beta_k T_s}}{2}, \tag{31a}$$

$$\sigma_k = \rho_k + e^{-\beta_k T_s}, \tag{31b}$$

where

$$\alpha_k = \frac{\underline{\chi}|S_k| - \underline{\boldsymbol{\tau}}_s(1 - |S_k|)}{m}, \qquad \beta_k = \frac{\overline{\chi}|S_k| - \overline{\boldsymbol{\tau}}_s(1 - |S_k|)}{m},$$

being

$$\boldsymbol{\tau}_s = -\frac{\log(\kappa\%)}{T_{sett,\kappa\%}}, \qquad \chi = \frac{\underline{\boldsymbol{\tau}}_s - \overline{\boldsymbol{\tau}}_s}{2} \pm p.$$

The term $S_k = \{k \in \{1, \dots, 2^{n_\Psi}\} : mod(j, 2^{n_\Psi}) \in \{1, \dots, 2^{n_\Psi - 1}\}\}$, being $|S_k|$ its cardinality, and the user-defined variable p determine the overlapping between fastest and slowest LMI regions. Note that all these regions are defined such that closed-loop system poles lie in the Right-Half Plane (RHP) of the discrete complex plane to avoid undesired oscillatory behaviours (Isermann, 2013).

The LMI framework gives a general description of regions in the complex plane under the definition of $\mathbb{D}$-stabilisation (Chilali, Gahinet, & Apkarian, 1999). The $\mathbb{D}_{c,k}$ circular regions considered in the shifting strategy are characterised by matrices

$$L_{c,k} = \begin{bmatrix} -\rho_k & \sigma_k \\ \sigma_k & -\rho_k \end{bmatrix}, \qquad M_{c,k} = M_c = \begin{bmatrix} 0 & 1 \\ 0 & 0 \end{bmatrix}.$$

Thus, under the shifting control strategy, LQR design problem (Ostertag, 2011) defined $\forall \vec{i} \in \mathbb{I}_{(2,2^{n_\Phi})}$ has to be stated $\forall k = 1, \dots, 2^{n_\Psi}$ as follows:

$$\begin{bmatrix} -Y & YA_{i_1}^T - W_{i_1,k}^T B_{i_2}^T & YH_c^T & W_{i_1,k}^T \\ (*) & -Y & 0 & 0 \\ (*) & 0 & -I & 0 \\ (*) & 0 & 0 & -R_c^{-1} \end{bmatrix} < 0, \tag{32a}$$

$$\begin{bmatrix} \gamma_c I & I \\ I & Y \end{bmatrix} > 0 \tag{32b}$$

and the corresponding LMI pole placement conditions have to be included intro the control synthesis problem:

$$\begin{aligned} &L_{c,k} \otimes Y + M_c \otimes (A_{i_1} Y - W_{i_1,k} B_{i_2}) \\ &\quad + M_c^T \otimes (A_{i_1} Y - W_{i_1,k} B_{i_2})^T < 0, \end{aligned} \tag{33}$$

being $K_{fb,nm} = W_{n,m} Y^{-1}$.

Remark 5. The presented shifting approach assumes that the sum of gravity and exogenous force effects to be compensated will not be greater than the actuator saturation limits, which will limit their operation to the linear region. Although it might seem like a strong assumption to be made, robotic manipulators are generally designed towards increasing their payload-weight ratio, i.e. reducing its inertia while increasing the maximum load it can handle. Also, the design process of robotic manipulators generally considers the maximum forces to be exerted by the robot according to their context of operation.

Remark 6. Under the Shifting Control paradigm, the definition given in Eq. (23) for the Feedforward Scaling matrix $S(\Phi)$ has to be slightly modified to include terms $K_{fb,nm}$, akin to reformulation of the state-feedback control law in Eq. (28) from Eq. (22).

Remark 7. Design problems of the observer (RUIO) and control strategy (State-Feedback Shifting Controller) have been considered separately, which is customary in control implementation problems, as e.g. in Rotondo, Nejjari, and Puig (2013). However, the stability guarantees would be only guaranteed either by proving the separation principle or considering a joint design, being any of these two options investigated in a future research.

5.3. Polya's theorems formulation for the polytopic state-feedback shifting controller

The LPV description given in Eq. (5) sets an input matrix B function of Φ, which under the polytopic approach depicted in Eq. (8) corresponds to a set of B_n matrices. Thus, conditions from Eq. (32a) including the closed-loop form of the system, involve the combination of every B_n with all W_n or $W_{n,m}$, meaning that each gain has to be robust with respect to every possible input matrix, increasing the overall conservatism of the design problem. Moreover, control shifting approach includes additional pole placement conditions from Eq. (33), which involve same combinations. Similarly to Section 4.3, we can relax the LMI conditions on the design process applying Polya's theorems. Therefore, for $r \geq 2$ for conditions from Eqs. (32a) and (33) we obtain the following sufficient conditions $\forall \vec{i} \in \mathbb{I}^{+}_{(r,2^{n_\Phi})}$ and $\forall k = 1, \dots, 2^{n_\Psi}$:

$$\sum_{\vec{j} \in \mathcal{P}(\vec{i})} \begin{bmatrix} -Y & Y A_{j_1}^T - W_{j_1,k}^T B_{j_2}^T & Y H_c^T & W_{j_1,k}^T \\ (*) & -Y & 0 & 0 \\ (*) & 0 & -I & 0 \\ (*) & 0 & 0 & R_c^{-1} \end{bmatrix} < 0 \tag{34a}$$

$$\sum_{\vec{j} \in \mathcal{P}(\vec{i})} L_{c,k} \otimes Y + M_c \otimes (A_{j_1} Y - W_{j_1,k} B_{j_2}) + M_c^T \otimes (A_{j_1} Y - W_{j_1,k} B_{j_2})^T < 0. \tag{34b}$$

Remark 8. In the controller synthesis problem, a common variable Y is used for the candidate Lyapunov function, instead of a polytopic set as with the RUIO. Although it increases the degree of conservatism, it will also add an additional combinatorial index to the existing one due to variant B. Polya's theorems allow a definition for any r-degree combination, but we have preferred to provide a unique application case to avoid misunderstandings.

6. Case study

In this section, the implementation process of the control architecture presented in this paper is described for the TIAGo head example, providing general guidelines to be applied for any N-DoF mechanism with rotational joints. First, the design problem of both the shifting controller and RUIO will be stated, endorsing made choices. Then, simulation results are provided for a real scenario involving TIAGo in a environment simulated in ROS.

6.1. Design problem

The polytopic set of state–space matrices for the N-DoF manipulator system has been discretised using the Zero-order Hold (ZoH) method, considering the discretisation behaviour of Analog–Digital conversion in both sensing and acting devices (Toth et al., 2010). Sampling time T_s has been chosen according to the required execution and communication times of the platform for a *worst-case scenario*.

Table 3
LMI circular regions radii ρ and centres σ for observer and control synthesis problems of the TIAGo head system.

Problem	ρ	σ
Shifting control	[0.0243,0.0246,0.0246,0.0249]	[0.9490,0.9610,0.9610,0.9732]
RUIO	0.2890	0.2990

TIAGo head uses Dynamixel servomotors from ROBOTIS,[4] specifically MX-64 model, which features current-based torque control. Executing the code in MATLAB (2016b version), using the available Dynamixel SDK library and considering TTL serial communication, the execution time per cycle has been determined to be below 0.5 ms under these conditions. Therefore, $T_s = 10$ [ms] has been used, where idle time contemplates the simultaneous execution of other processes that would increase computation time, as e.g. an object tracking algorithm.

Considering the overall control architecture, RUIO synthesis problem has to be extended with a $\mathbb{D}$-stabilisation constraint such that there does not exist any dynamical coupling between closed-loop system and observer. Therefore, dominant poles of the RUIO have been set to be at least 10 times faster than the fastest pole of the shifting controller. Following $\mathbb{D}$-stabilisation definition, LMI constraint is stated for N_n matrix, as it determines the error dynamics of the RUIO:

$$L_o \otimes X_n + M_o \otimes N_n X_n + M_o^T \otimes X_n N_n^T < 0, \tag{35}$$

where

$$L_o = \begin{bmatrix} -\rho_o & \sigma_o \\ \sigma_o & -\rho_o \end{bmatrix}, \qquad M_o = \begin{bmatrix} 0 & 1 \\ 0 & 0 \end{bmatrix}.$$

define a circular region, being σ_o and ρ_o determined according to aforementioned criterion after the controller synthesis problem, and recalling that they should lie on the RHP. For the TIAGo head system, these values have been included in Table 3.

A quadratic criterion has been introduced in both controller and observer design, being upper bounded by parameter γ for any reachable state, according to matrices Q and R. Optimality of the solution is obtained through the minimisation of γ such that the set of LMI constraints holds. Hence, synthesis problems have been stated as follows:

Optimal RUIO Design

Given	Q_o, R_o, L_o, M_o
minimise	γ_o
subject to	(21), (19b), (19c), (35)

Shifting Controller Design

Given	Q_c, R_c, M_c and $L_{c,k}$ $\forall k = 1, \dots, 2^{n_\Psi}$
minimise	γ_c
subject to	(34a), (34b), (32b)

To achieve noise reduction effects for the RUIO, Q_o and R_o have been defined according to sensor and process noise. For the TIAGo head system sensors, noise follows a zero-mean Gaussian distribution, with standard deviations $\sigma_p = 1 \cdot 10^{-4}$ [rad] and $\sigma_v = 3 \cdot 10^{-4}$ [rad/s] for joint position and velocity, respectively. In the shifting controller design Q_c and R_c are defined according to a weighted Bryson's rule given a set of maximum admissible values for actions and states. Weights δ_i have been obtained through a tuning process aimed at reducing oscillatory behaviours in the system response to step references. These matrix definitions for the TIAGo head example have been gathered in Table 4.

Regarding the shifting strategy, closed-loop settling time for $\kappa = 2\%$ has been chosen to lie in [0.5,20] [s], defining through Eqs. (31) sets ρ_k

[4] Dynamixel Actuator Series from ROBOTIS: http://en.robotis.com/model/page.php?co_id=prd_dynamixel (Accessed August 18, 2021).

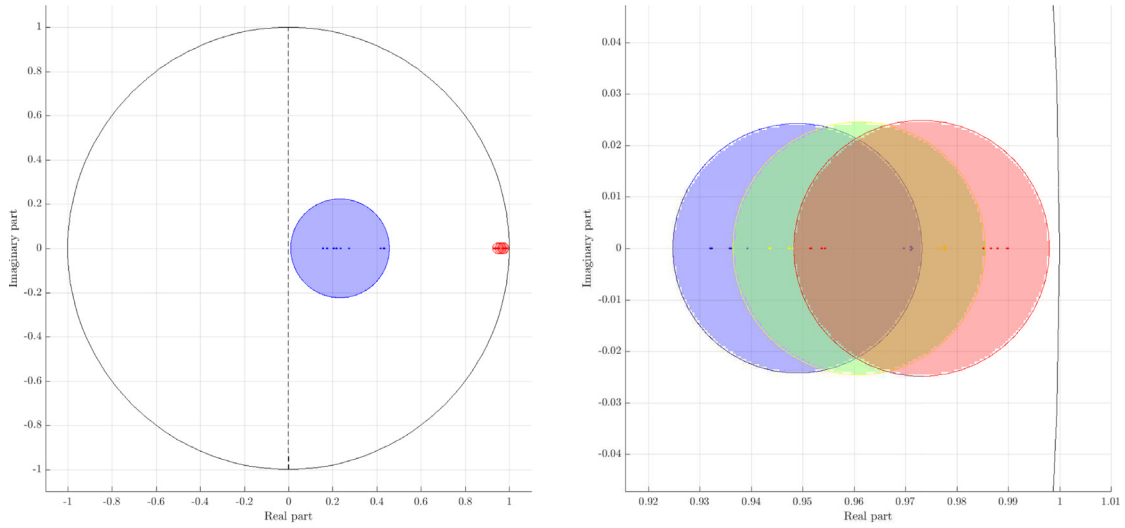

Fig. 4. Placement of poles and defined LMI regions for closed-loop system with shifting state-feedback control (red) and RUIO (blue) solutions in the complex plane (a), and a detail of the closed-loop system placement of poles and LMI regions corresponding to the shifting strategy (b). (For interpretation of the references to colour in this figure legend, the reader is referred to the web version of this article.)

Table 4
Definition of tuning matrices Q and R for RUIO and shifting control synthesis problems of the TIAGo head system.

Matrix	Definition
R_o	$\text{diag}(3^2,\ 1^2,\ 1^2)\cdot 10^{-8}$
Q_c	Δ_{Q_c} =diag(0.99, 0.99, 0.01, 0.01) $\overline{D}_{Q_c} = \text{diag}(1/3^2,\ 1/3^2,\ 1/1.31^2\ 1/1.05^2$
R_c	$\Delta_{R_c} = \text{diag}(0.9,\ 0.9)$ $\overline{D}_{R_c} = \text{diag}(1/6^2,\ 1/6^2)$

Table 5
Number of LMI constraints for the control synthesis problem of the TIAGo head system, regarding different formulations and performance constraints. In bold, the corresponding one to the complete scheme.

Formulation		Def.	Pole plac.	Main		Total
				LMI	Equal.	
Standard	Stability	3	16	16	–	35
Polya's ($r = 3$)	LQR & No shifting	3	20	20	–	43
	LQR & Shifting	**3**	**68**	**68**	–	**139**

Table 6
Number of LMI constraints for the RUIO synthesis problem of the TIAGo head system, regarding different formulations and performance constraints. In bold, the corresponding one to the complete scheme.

Formulation		Def.	Pole plac.	Main		Total
				LMI	Equal.	
Standard	Stability	4	4	16	4	28
Polya's ($r = 5$)	**LQR**	**5**	**4**	**57**	**4**	**70**

and σ_k of the four LMI regions for the TIAGo head case, also included in Table 3. Lower values of p determine greater overlapping between regions in the discrete complex plane, and for the considered system a maximum of $p = -1.3$ has been found.

LMI conditions have been stated using YALMIP toolbox (Löfberg, 2004) for MATLAB, and solved by the Semi-Definite Programming (SDP) algorithms provided by MOSEK.[5] Feasible solutions have been found in both cases, and the number of LMI constraints has been detailed for the TIAGo head case in Tables 5 and 6 for the Shifting Control and RUIO Designs, respectively. It should be pointed out that in these Tables, column "Def." considers all the constraints regarding the definition of the problem and/or the bound of γ, "Pole plac." for those defining LMI regions, and "Main" for the ones that determine the overall objective of the design, e.g. stability, optimal conditions and/or specific conditions linked to the structure definition, distinguishing between LMI and equality ("Equal.") constraints. These tables additionally include the same information for each problem with and without the application of Polya's theorems and regarding different performance constraints.

Obtained solution for the TIAGo head has been graphically reproduced through the representation of chosen LMI regions and the corresponding poles. Fig. 4(a) distinguishes the LMI regions imposed for the observer (blue) and closed-loop system (red) within the unit circle. Shifting strategy is detailed in Fig. 4(b), where the distribution of obtained 4 LMI regions (2^{n_u}) is depicted.

6.2. Simulation results

In this part, we focus on key aspects of the presented control architecture through different scenarios to assess its overall performance in the joint tracking problem. All of them correspond to different settings in the GAZEBO environment, where the TIAGo tracks an ArUco cube marker[6] by moving its head (which embeds a RGB-D camera) in the presence of exogenous forces (Fig. 5). Results provided in this part consist on combinations of angular trajectories (Step References, Curve References) and exogenous force behaviours (Mass Force, Variant Force,

[5] MOSEK optimisation software: https://www.mosek.com/ (Accessed August 18, 2021).

[6] ArUco: a minimal library for Augmented Reality applications based on OpenCV: https://www.uco.es/investiga/grupos/ava/node/26 (Accessed August 18, 2021).

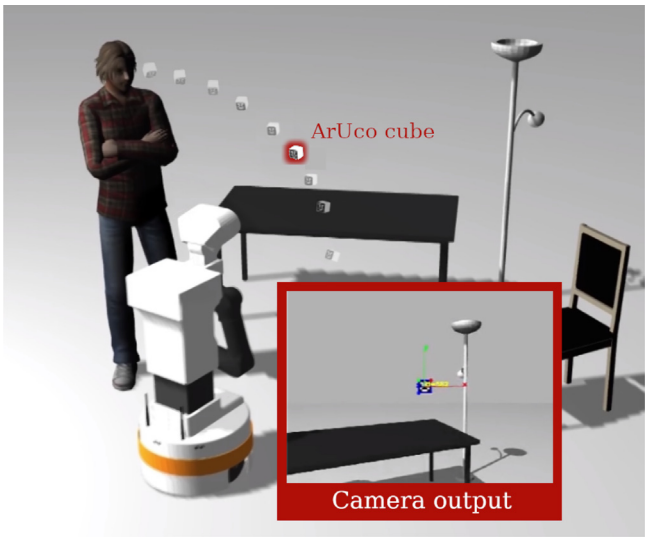

Fig. 5. Gazebo environment for the cube following task, together with the RGB-D camera output and the ArUco marker detection.

Half-Sinus Force), which are thoughtfully described in Appendix D. Additionally we have included a video that shows the performance of our approach ("Polytopic State-Feedback Shifting Control with Active Compensation") against the default joint-independent PD control, which can be also found in the related website.[7]

Remark 9. It should be pointed out that under the same force behaviour, different control strategies and trajectories influence its effect, as exerted joint torques by the exogenous force depend on the relative distances to joint axes, that change according to angular positions.

6.2.1. Noise effect reduction

The first scenario is built for Curve References and Variant Force to evaluate the noise reduction effect of the Optimal RUIO formulation. For the TIAGo case, noise is propagated from the estimation of $\hat{\dot{q}}_1$ to the state-feedback control and active compensation, i.e. the input action to the system, amplifying its effect on measured variables, used in the RUIO estimation at next time step. Fig. 6 shows a side-by-side comparison between solutions under the same conditions, showing the improvement in estimating both $\hat{\dot{q}}_1$ and torque exerted in Pan Joint $\hat{\tau}_{\mathcal{F},1}$, where the noise effect is most significant. Nevertheless, RUIO estimation at time instant k is based on current system output, unlike classical Kalman Filters where it is done for output at $k-1$. Thus, noise reduction cannot be as effective for RUIO as it is for Kalman Filter, as measurement noise is directly injected into state estimation without being filtered out by observer dynamics.

6.2.2. Overall performance

Performance of the complete control scheme is evaluated on Curve References for Mass and Variant Force scenarios. To validate our approach, we have included in these experiments a comparison against two variations:

- **EKF variation:** The complete control scheme, except for the RUIO, replaced by an Extended Kalman Filter (EKF). As aforementioned, it is considered in the unknown disturbance rejection literature as the state-of-art technique. Using this approach, state–space is augmented to include the disturbance effects into the observer model, which requires to *a-priori* assume its dynamic behaviour. In discrete-time scenarios, the rate of change of the disturbance in EKF is assumed to be constant throughout the operation, i.e. $\dot{\tau}_{\mathcal{F}}(t) = 0$ (Mohammadi et al., 2013), which has been also considered for these experiments.
- **PD and Active Compensation variation:** using the estimation of the RUIO and the disturbance compensation mechanism, State-feedback Shifting controller is substituted by an independent-joint PD controller. This constitutes the *off-the-shelf* solution for regulation tasks, and is the one implemented as the pose control strategy for the TIAGo head system. Current PD gains embedded in joint actuators are presented in Table 7.

Table 7
Actuator PD gains for TIAGo head system.

Joint	P Gain	D Gain
q_1	1	32
q_2	5	34

Table 8
Root Mean Squared Error (RMSE) (in [°]) for compared control strategies under different force scenarios.

Scenario	Joint	Complete scheme	EKF	PD & Act. Comp.
No force	q_1	1.5413	1.3146	**0.1192**
	q_2	1.3196	1.2035	**0.1545**
Mass applied	q_1	1.3863	1.3166	**0.1078**
	q_2	**1.3085**	2.2115	1.5209
Variant force	q_1	**1.9658**	3.8871	1.9888
	q_2	**2.8069**	6.0832	4.9082

Figs. 7 and 8 include the results for considered force scenarios, summarised in Table 8 using the Root Mean-Squared Error (RMSE) over the whole simulation together with its value when there is not an exogenous force acting on the system. Under the Mass Force, applied in $t \approx [25\text{–}35]$ [s] as it can be seen in Fig. 7(c), only q_2 is affected, and except both the Complete Design and the EKF variation are able to compensate for the exogenous force effects that are rejected during this time. It should be pointed out that the force effect on the EKF variation produces a higher deviation from the reference trajectory when the force is firstly applied at 25 [s] and released at 35 [s], approximately. For the Variant Force case depicted in Fig. 8, differences between the methods become more significant, and the Complete Scheme presented in this paper outperforms the variations of the method. Overall, PD control with Active Compensation presents less deviation than the EKF variation, which even reaches the upper q_1 limit in the interval $t = [20, 25]$ [s]. Greatest fluctuations of the EKF variation correspond to $t \approx [18\text{–}28]$ [s], when the exogenous force has a magnitude peak, as it can be seen in Fig. 8(c). This arises from the EKF design, which requires assuming the dynamics of the unknown disturbance, constant in these experiments. When a significant mismatch with its real behaviour occurs, the compensation of the estimated effects hinders the rejection capabilities of the control scheme.

To further analyse the differences between the EKF and RUIO, Table 9 includes the RMSE for $\dot{q}_1$, $\tau_{\mathcal{F},1}$ and $\tau_{\mathcal{F},2}$ for the Variant Force case. RUIO has lower RMSE in all estimations, being one order of magnitude lower than EKF for the exogenous force torques. Together with the previous results, this highlights the importance of avoiding any *a-priori* assumption on the disturbance behaviour, moreover if it is meant to be rejected by a feedforward compensation strategy. Thus, using RUIO has been proved to be a more suitable option for disturbance rejection problems than state-of-art EKF technique.

6.2.3. Actuator saturation

Finally, Shifting control is evaluated for Step References and Half-Sinus Forces in order to emulate an scenario where the required control torque is close to actuator saturation limits. The complete scheme featuring the shifting strategy is compared against two *static* state-feedback

[7] http://www.iri.upc.edu/people/asanmiguel/Projects/DO_LPVShift/.

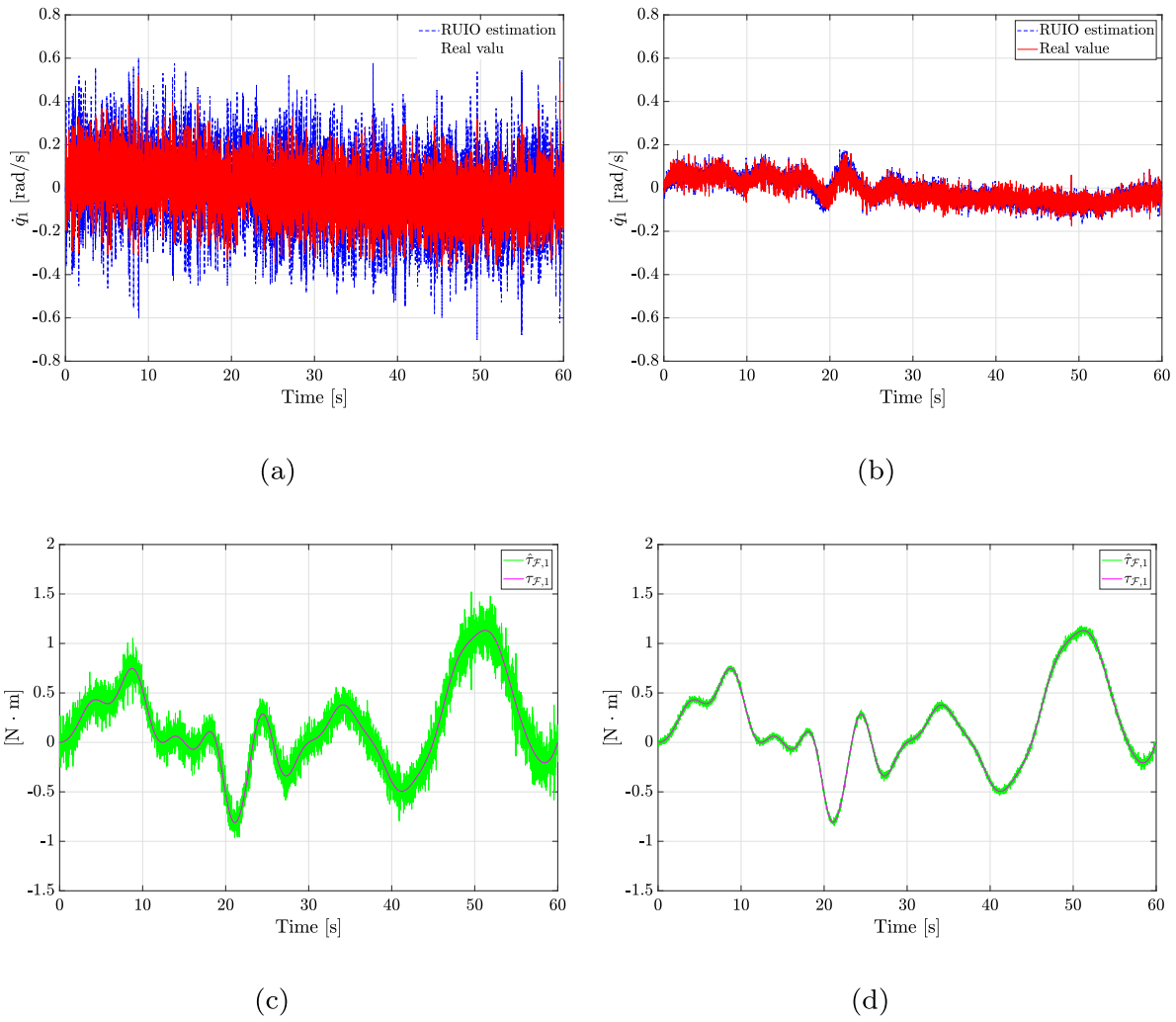

Fig. 6. Evolution of $\dot{q}_1$ and $\tau_{F,1}$ and their estimation for RUIO standard formulation (a,c) and optimal one for noise reduction (b,d) under the Variant Force. (For interpretation of the references to colour in this figure legend, the reader is referred to the web version of this article.)

Table 9
Root Mean Squared Error (RMSE) of estimated values given RUIO and EKF (for the same control strategy) under the Variant Force scenario, excluding measurement noise effects.

Variable	RUIO	EKF
$\hat{\dot{q}}_1$ [°/s]	**0.7528**	0.8731
$\hat{\tau}_{F,1}$ [N m]	**0.0043**	0.0663
$\hat{\tau}_{F,2}$ [N m]	**0.0041**	0.0665

Table 10
Root Mean Squared Error (RMSE) (in [°]) for compared shifting and pole placement strategies under different force scenarios.

Scenario	Joint	Complete scheme	Fast cont.	Slow cont.
No force	q_1	17.7408	**15.6746**	32.1372
	q_2	11.1072	**9.9150**	19.5654
Half-Sinus force	q_1	19.8564	**15.6929**	33.2427
	q_2	12.4489	**9.9723**	21.2979

controllers, designed also according to their settling time for a single LMI circular Region: a slower controller with $T_{sett,2\%} = [0.5, 20]$ [s] and a faster one with $T_{sett,2\%} = [0.5, 1]$ [s]. Fig. 9 shows the Pan trajectory together with a flag signal to indicate whether joint actuator saturates or not, for the complete scheme, and the slower and faster controllers. Table 10 presents the RMSE over the whole simulation for all these control approaches under aforementioned scenario and without an exogenous force. Faster controller reaches saturation limits in Pan Joint for 0.07 [s] (Fig. 9(c)) when the Half-Sinus Force is applied, while the complete shifting controller does for 0.01 [s] (Fig. 9(a)). Looking at the RMSE values of each strategy it can be seen that while Fast controller presents similar values in both scenarios, complete scheme ones slightly increase under the Half-Sinus Force, i.e. there exist a relaxation in the tracking task to deal with the active compensation while avoiding actuator saturation. Note that for the slow controller actuator saturation is reached for 0.27 [s] (Fig. 9(b)), although it presents the slower response time among the compared strategies. As it has been aforementioned, exerted torques depend on the manipulator pose, which determines the relative distances between the point of application of the force and joint axes. Thus, when the applied force gets closer to its maximum value, slow controller drives the system to an angular position where force is applied further from the joint axes, increasing its exerted torque. Additionally Fig. 10 has been included to visualise the Shifting strategy in this scenario, including the evolution of shifting variables Ψ_i and weights ν_m.

7. Conclusions and future work

Existing joint-independent PD control in the TIAGo head system cannot deal with exogenous forces in a regulation task. The approach proposed in this paper successfully tackles this problem, as provided

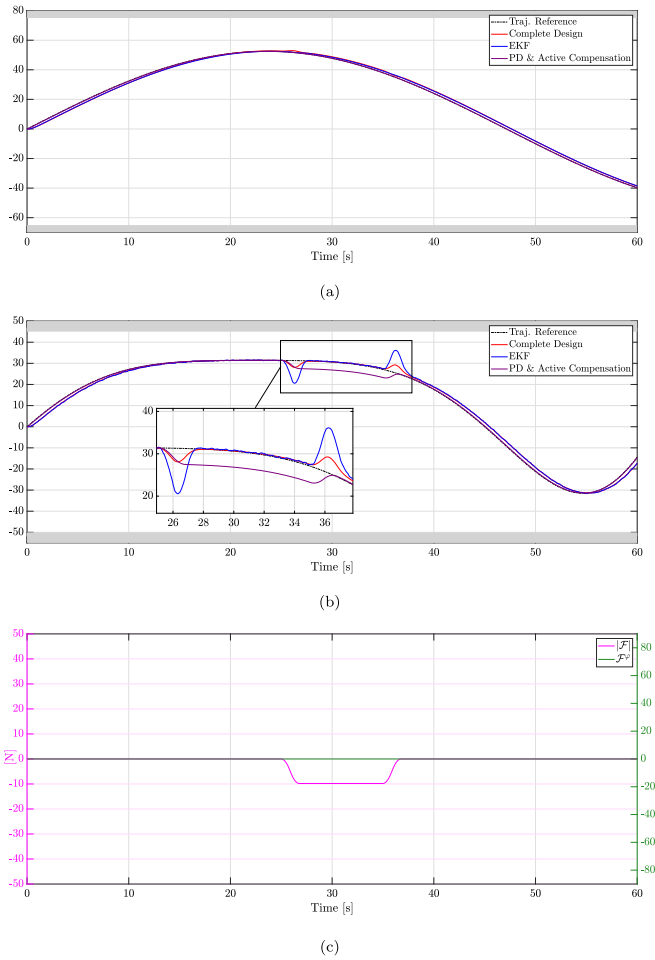

Fig. 7. Desired trajectories and evolution of q_1 (a) and q_2 (b) under the Mass Force scenario, depicted in terms of magnitude and orientation (c), for compared control strategies. Grey areas in (a,b) represent the physical joint limits. (For interpretation of the references to colour in this figure legend, the reader is referred to the web version of this article.)

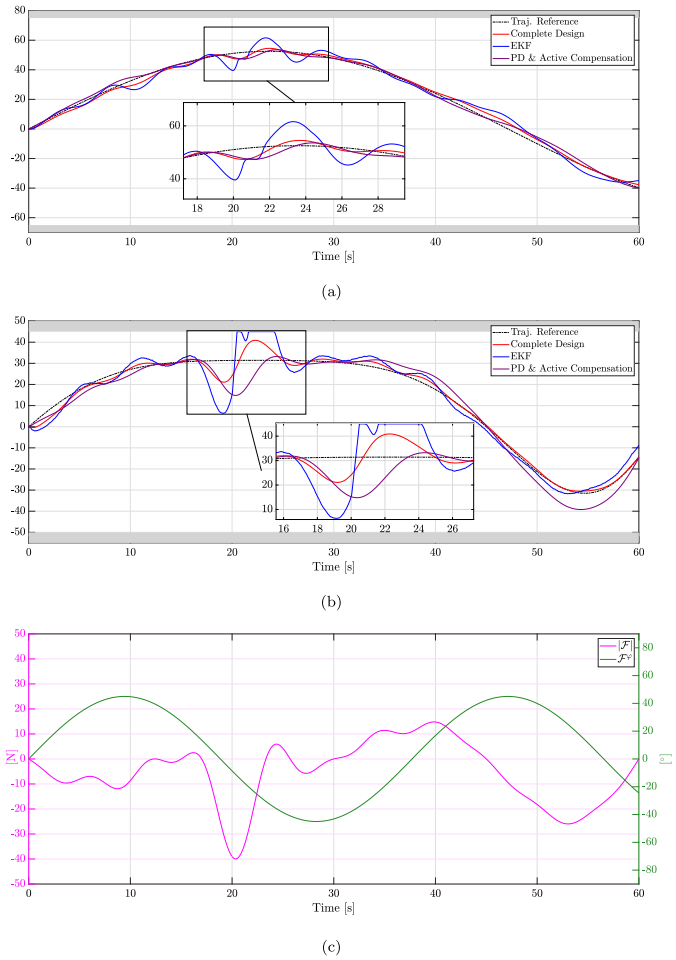

Fig. 8. Desired trajectories and evolution of q_1 and q_2 (a,b) under the Variant Force scenario, depicted in terms of magnitude and orientation (c), for compared control strategies. Grey areas in (a,b) represent the physical joint limits. (For interpretation of the references to colour in this figure legend, the reader is referred to the web version of this article.)

results in a realistic simulation case study. Moreover, guidelines to be applied on any N-DoF robotic manipulator are given for the design and implementation phases. Embedded optimal conditions for the RUIO represent an improvement in the noise reduction properties of the observer, enhancing the overall performance. Shifting approach allows to modify system response through the placement of closed-loop poles in LMI regions, which has been shown to help avoiding actuator saturation when actively compensated effects are close to input limits. The application of Polya's theorems has been used to reduce the conservatism of both control and RUIO synthesis problems through the definition of sufficient constraints, such that feasible solutions can be found even under highly conservative constraint and definitions.

In future works we will aim at (1) extending the system analysis, mainly regarding stability of the RUIO and Shifting controller together and (2) adapting this control architecture for new scenarios and robotic manipulators with more than 2-DoF operating in a task-relevant space. One interesting research line that could be followed is to consider a disturbance corresponding to a force exerted by a human, either accidentally or not. This consideration will require far more complex reaction and adaptation mechanisms from the control architecture, that might be integrated through the presented gain shifting paradigm. Furthermore, an in-depth comparison against other non-linear control strategies is needed, specially regarding their suitability for implementation in robotic platforms.

Declaration of competing interest

The authors declare that they have no known competing financial interests or personal relationships that could have appeared to influence the work reported in this paper.

Acknowledgement

This work is supported by the Spanish State Research Agency through the María de Maeztu Seal of Excellence to IRI MDM-2016-0656.

Appendix A. Modelling assumptions for the TIAGo head system

To obtain the formulation of Eq. (1) for the TIAGo head system the following customary guidelines have been considered to formulate its model as :

- Base frame (Link 0) is placed at the top part of TIAGo torso, which features a vertical movement. Considering that is not moving during the trajectory following task, head base frame has been set as fixed.
- Each link is considered as a rigid body, whose mass distribution is characterised by the position of its Centre of Gravity (CoG), being its inertia tensor and mass referred to it. We use the parameters

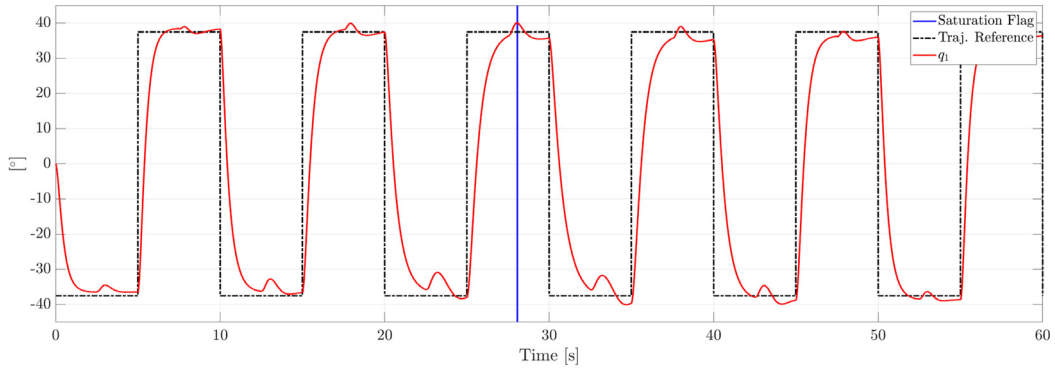

(a)

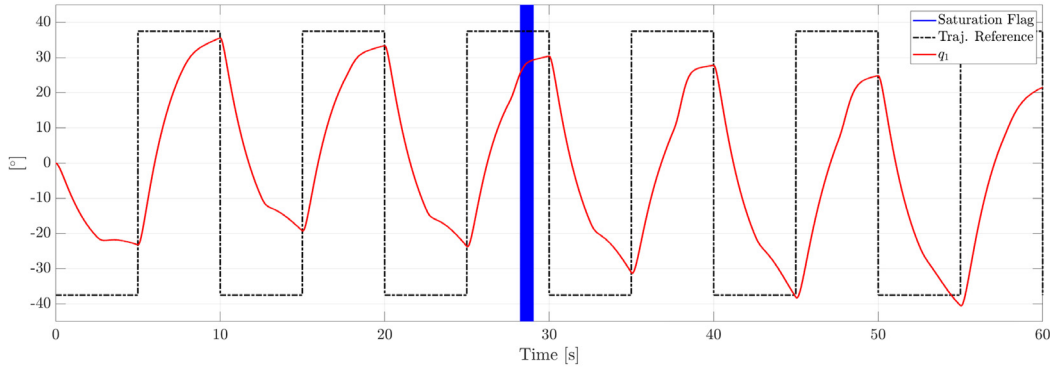

(b)

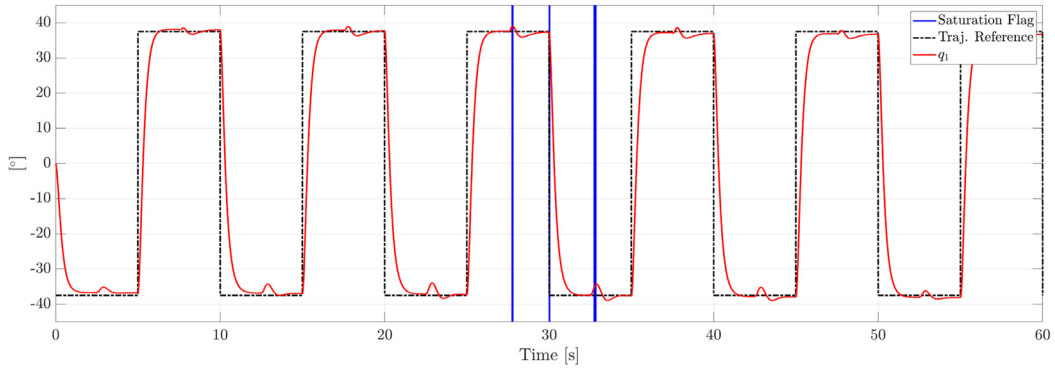

(c)

Fig. 9. Evolution of q_1 under the Half-Sin Force scenario, together with the saturation limit flag (blue regions), using the designed shifting (a), the slow (b) and the fast (c) controller designs. (For interpretation of the references to colour in this figure legend, the reader is referred to the web version of this article.)

as defined by PAL Robotics in the ROS simulation environment, listed in Table 1 and included in Fig. 2. On the inertia tensors for both links, off-diagonal terms are negligible with respect to diagonal ones (by a factor of 10^{-4}), and therefore have been considered as null.

- The pose depicted in Fig. 2 is the zero-angle configuration of the head system, being aligned axis ${}^2\hat{X}_2$ and ${}^1\hat{X}_1$ with ${}^0\hat{X}_0$; and ${}^2\hat{Y}_2$ and ${}^1\hat{Z}_1$ with ${}^0\hat{Z}_0$.
- External forces and torques acting on the head system have not been considered for its dynamic characterisation.

Appendix B. Proof of Proposition 1

Considering the set

$$\mathbf{P} = \{P_1, \dots, P_{2^{n_\Phi}}\};\ P_n \in \mathbb{R}^{n_x \times n_x} \mid P_n = P_n^T > 0 \quad \forall n = 1, \dots, 2^{n_\Phi}$$

for the candidate polytopic Lyapunov function

$$\mathbf{N}(e(k)) = \sum_{n=1}^{2^{n_\Phi}} \mu_n(\boldsymbol{\Phi})\, e(k)^T\, P_n\, e(k),$$

applying the Kalman filter Riccati equation to the RUIO description given in Eq. (15), the following inequality can be obtained $\forall \vec{i} \in \mathbb{I}_{(2,2^{n_\Phi})}$

$$N_{i_1}^T P_{i_2}\, N_{i_1} - P_{i_1} + Q_o + K_{i_1}\, R_o\, K_{i_1}^T < 0.$$

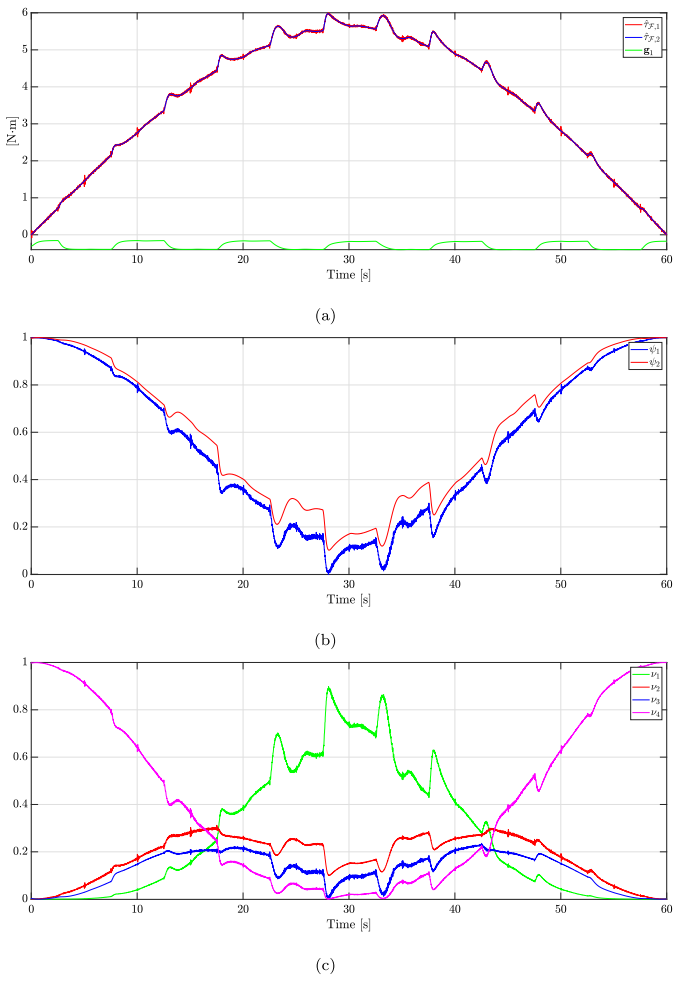

Fig. 10. Evolution of estimated torques exerted by the exogenous force $\hat{\tau}_{\mathcal{F},i}$ and gravity effects $\hat{\mathbf{g}}$ (a), shifting variables Ψ_i (b) and the associated weights ν_m (c) under the Half-Sin Force scenario, for the complete control design. (For interpretation of the references to colour in this figure legend, the reader is referred to the web version of this article.)

Multiplying both sides by $X_{i_1} = P_{i_1}^{-1}$ and introducing the variable change $W_{i_1} = X_{i_1} K_{i_1}$ leads to

$$-X_{i_1} - [(N_{i_1}^T X_{i_1})^T \quad (H_o X_{i_1})^T \quad W_{i_1}] \begin{bmatrix} -X_{i_2}^{-1} & 0 & 0 \\ 0 & -I & 0 \\ 0 & 0 & -R_o \end{bmatrix} \begin{bmatrix} N_{i_1}^T X_{i_1} \\ H_o X_{i_1} \\ W_{i_1}^T \end{bmatrix} < 0,$$

Applying Schur complement lemma, we obtain

$$\begin{bmatrix} -X_{i_1} & X_{i_1} N_{i_1} & X_{i_1} H_o^T & W_{i_1} \\ (*) & -X_{i_2} & 0 & 0 \\ (*) & 0 & -I & 0 \\ (*) & 0 & 0 & -R_o^{-1} \end{bmatrix} < 0.$$

and considering $S_n = X_n E$ results in Eq. (19b), following the standard design of the RUIO.

Lyapunov matrix set **P** is bounded for all the reachable state domain according to the optimality criterion J_o such that

$$\sum_{n=1}^{2^{n_\Psi}} \mu_n(\Psi)\, P_n < \gamma_o I.$$

As aforementioned, multiplying at both sides by the change of variable $X_n = P_n^{-1}$ leads to

$$\gamma_o I - I\, X_n^{-1}\, I > 0,$$

from which Eq. (19c) is obtained after applying the Schur complement lemma.

Appendix C. Application of Polya's theorem on combinatorial LMIs

Assessing positive-definiteness of the symmetric matrix $\mathcal{Q}_{i_1 i_2}$ for a polytopic LPV system of n_{Φ} scheduling variables implies:

$$\Xi = \sum_{i_1=1}^{2^{n_\Phi}} \sum_{i_2=1}^{2^{n_\Phi}} \mu_{i_1}(\Phi)\, \mu_{i_1}(\Phi)\, x^T\, \mathcal{Q}_{i_1 i_2}\, x > 0, \qquad \forall\, i \in \mathbb{I}^+_{(2,2^{n_\Phi})} \tag{C.1}$$

According to Sala and Arino (2007), application of Polya's theorems sets that for a fixed $r \geq 2$, on the positive-definiteness conditions from Eq. (C.1), constraints defined as

$$\tilde{\mathcal{Q}}_{\vec{i}} = \sum_{\vec{j} \in \mathcal{P}(\vec{i})} \mathcal{Q}_{j_1 j_2} > 0, \qquad \forall\, \vec{i} \in \mathbb{I}^+_{(r,2^{n_\Phi})} \tag{C.2}$$

where $\mathcal{P}(\vec{i})$ denotes the permutation set of multi-index $\vec{i}$,

$$\mathbb{I}^+_{(r,h)} = \{\vec{i} \in \mathbb{I}_{(r,h)} \mid i_m \leq i_{m+1},\, m = 1, \ldots, r-1\}$$

are sufficient for positivity of Ξ. Note that this formulation is valid for both continuous and discrete-time system forms as it does not impose any form of $\mathcal{Q}_{j_1 j_2}$. Also, although it has been defined for positive-definitive assessment, it can be equivalently used for negative case.

Appendix D. Simulation scenarios

- **Joint Angle Trajectories**

  T.1 Step References given between two symmetric angular positions, such that there exist an phase offset between joints to stress the dynamical coupling effects. For the TIAGo head case, Pan angle trajectory is defined for $\mp\, 0.5\, \bar{q}_1$ and Tilt one for $\pm\, 0.5\, \bar{q}_2$, with a period of 10 [s] and existing a 5 [s] offset $(\pi/2)$ between them.

  T.2 Curve References to mimic trajectories given by an upper layer to the control architecture, as e.g. path generator via a set of points. In this case

  $$q_{1,ref}(t) = 0.7\, \bar{q}_1\, \sin(0.04t),$$
  $$q_{2,ref}(t) = 0.7\, \bar{q}_2\, \sin(0.08t - 26 \cdot 10^{-4}\, t^2),$$

  evaluated each time step k as $t = k\, T_s$.

- **Exogenous force behaviours**. Forces have been considered to be exerted on the CoG of the second link, defined as function of a magnitude $|\mathcal{F}|$ and orientation $\mathcal{F}^{\varphi}$ w.r.t. the vertical axis of the manipulator base.

  F.1 Mass Force, i.e. the force corresponding to a mass attached to the robot, addressing the issue that motivated the application of presented approach to the TIAGo head system. Force orientation is constant and equal to zero and the magnitude corresponds to a trapezoidal *rounded-edge* signal with a 1 [s] rise time to emulate the mass placement effect. For these simulations, placed mass is of 1 [kg].

  F.2 Variant Force in both magnitude and orientation, according to the following equations for the TIAGo case:

  $$|\mathcal{F}|(t) = 15 \cdot 10^{-2}(t-20) + 3\sin(t-20)/(t-20)\ \text{[N]}$$
  $$\mathcal{F}^{\varphi}(t) = 45\sin(0.17t)\ \text{[rad]}$$

  F.3 Half-Sinus Force in terms of magnitude, to assess control behaviour from zero to a maximum value. For the TIAGo head case, considering a constant orientation of -45 [°], the maximum force value has been set to 8.5 [N].

References

Agarwal, V., & Parthasarathy, H. (2016). Disturbance estimator as a state observer with extended Kalman filter for robotic manipulator. *Nonlinear Dynamics*, *85*(4), 2809–2825.

Alami, R., Albu-Schäffer, A., Bicchi, A., Bischoff, R., Chatila, R., De Luca, A., et al. (2006). Safe and dependable physical human-robot interaction in anthropic domains: State of the art and challenges. In *Proceedings of the 2006 IEEE/RSJ international conference on intelligent robots and systems* (pp. 1–16). IEEE.

Bae, H., & Oh, J.-H. (2017). Novel state estimation framework for humanoid robot. *Robotics and Autonomous Systems*, *98*, 258–275.

Bruzelius, F., Breitholtz, C., & Pettersson, S. (2002). LPV-based gain scheduling technique applied to a turbo fan engine model. In *Proceedings of the 2002 international conference on control applications (CCA), Vol. 2* (pp. 713–718). IEEE.

Chadli, M., & Karimi, H. R. (2012). Robust observer design for unknown inputs Takagi–Sugeno models. *IEEE Transactions on Fuzzy Systems*, *21*(1), 158–164.

Chilali, M., Gahinet, P., & Apkarian, P. (1999). Robust pole placement in LMI regions. *IEEE Transactions on Automatic Control*, *44*(12), 2257–2270.

Colomé, A., Planells, A., & Torras, C. (2015). A friction-model-based framework for reinforcement learning of robotic tasks in non-rigid environments. In *Proceedings of the 2015 IEEE international conference on robotics and automation (ICRA)* (pp. 5649–5654). IEEE.

Craig, J. J. (2009). *Introduction to robotics: Mechanics and control, 3/E*. Pearson Education India.

Ha, W., & Back, J. (2019). A robust tracking controller for robot manipulators: Embedding internal model of disturbances. In *Proceedings of the 2019 international conference on robotics and automation (ICRA)* (pp. 1162–1168). IEEE.

Hashemi, S. M., Abbas, H. S., & Werner, H. (2012). Low-complexity linear parameter-varying modeling and control of a robotic manipulator. *Control Engineering Practice*, *20*(3), 248–257.

He, W., Wang, T., He, X., Yang, L.-J., & Kaynak, O. (2020). Dynamical modeling and boundary vibration control of a rigid-flexible wing system. *IEEE/ASME Transactions on Mechatronics*, *25*(6), 2711–2721.

Isermann, R. (2013). *Digital control systems*. Springer Science & Business Media.

Kim, M., Kim, J. H., Kim, S., Sim, J., & Park, J. (2018). Disturbance observer based linear feedback controller for compliant motion of humanoid robot. In *Proceedings of the 2018 IEEE international conference on robotics and automation (ICRA)* (pp. 403–410). IEEE.

Kwiatkowski, A., Boll, M.-T., & Werner, H. (2006). Automated generation and assessment of affine LPV models. In *Proceedings of the 45th IEEE conference on decision and control (CDC)* (pp. 6690–6695). IEEE.

Löfberg, J. (2004). YALMIP: A toolbox for modeling and optimization in MATLAB. In *Proceedings of the 2004 international symposium on computer-aided control system design (CACSD), Vol. 3*, Taipei, Taiwan.

Mohammadi, A., Tavakoli, M., Marquez, H. J., & Hashemzadeh, F. (2013). Nonlinear disturbance observer design for robotic manipulators. *Control Engineering Practice*, *21*(3), 253–267.

Mohammed, S., Huo, W., Huang, J., Rifaï, H., & Amirat, Y. (2016). Nonlinear disturbance observer based sliding mode control of a human-driven knee joint orthosis. *Robotics and Autonomous Systems*, *75*, 41–49.

Ostertag, E. (2011). *Mono-and multivariable control and estimation: Linear, quadratic and LMI methods*. Springer Science & Business Media.

Ren, C.-E., Du, T., Li, G., & Shi, Z. (2018). Disturbance observer-based consensus control for multiple robotic manipulators. *IEEE Access*, *6*, 51348–51354.

Rotondo, D., Nejjari, F., & Puig, V. (2013). Quasi-LPV modeling, identification and control of a twin rotor MIMO system. *Control Engineering Practice*, *21*(6), 829–846.

Rotondo, D., Nejjari, F., & Puig, V. (2015). Design of parameter-scheduled state-feedback controllers using shifting specifications. *Journal of the Franklin Institute*, *352*(1), 93–116.

Rotondo, D., Puig, V., Nejjari, F., & Witczak, M. (2015). Automated generation and comparison of Takagi–Sugeno and polytopic quasi-LPV models. *Fuzzy Sets and Systems*, *277*, 44–64.

Ruiz, A., Rotondo, D., & Morcego, B. (2019). Design of state-feedback controllers for linear parameter varying systems subject to time-varying input saturation. *Applied Sciences*, *9*(17), 3606.

Sala, A., & Arino, C. (2007). Asymptotically necessary and sufficient conditions for stability and performance in fuzzy control: Applications of Polya's theorem. *Fuzzy Sets and Systems*, *158*(24), 2671–2686.

Shamma, J. S. (2012). An overview of LPV systems. In *Control of linear parameter varying systems with applications* (pp. 3–26). Springer.

Toth, R., Heuberger, P. S., & Van den Hof, P. M. (2010). Discretisation of linear parameter-varying state-space representations. *IET Control Theory & Applications*, *4*(10), 2082–2096.

Witczak, M. (2014). Fault diagnosis and fault-tolerant control strategies for non-linear systems. *Lecture Notes in Electrical Engineering*, *266*, 375–392.

Zhao, Z., Ahn, C. K., & Li, H.-X. (2019). Boundary antidisturbance control of a spatially nonlinear flexible string system. *IEEE Transactions on Industrial Electronics*, *67*(6), 4846–4856.

Zhao, Z., He, X., & Ahn, C. K. (2019). Boundary disturbance observer-based control of a vibrating single-link flexible manipulator. *IEEE Transactions on Systems, Man, and Cybernetics: Systems*, *51*(4), 2382–2390.

Zhao, Z., & Liu, Z. (2020). Finite-time convergence disturbance rejection control for a flexible Timoshenko manipulator. *IEEE/CAA Journal of Automatica Sinica*, *8*(1), 157–168.